horticulturae

MDPI

Article

Integrating Metabolomics, Physiology and Satellite Vegetation Indices to Characterize Dormancy Onset in Two Sweet Cherry Genotypes

Gabriela M. Saavedra [1,2,†], Luciano Univaso [3,†], Laura Sepúlveda [4,5], José Gaete-Loyola [1], Carlos Nuñez [6], Victoria Lillo-Carmona [5,7,8], Valentina Castillo [9], Francisco Zambrano [10] and Andrea Miyasaka Almeida [1,9,*]

1 Centro de Genómica y Bioinformática, Facultad de Ciencias, Ingeniería y Tecnología, Universidad Mayor, Huechuraba 8580745, Santiago, Chile; gabriela.saavedrao@mayor.cl (G.M.S.); jose.gaetelo@umayor.cl (J.G.-L.)
2 Programa de Doctorado en Genómica Integrativa, Vicerrectoría de Investigación, Universidad Mayor, Huechuraba 8580745, Santiago, Chile
3 Bionostra Chile Research Foundation, Almirante Lynch 1179, San Miguel 8920033, Santiago, Chile; luciano.univaso@gmail.com
4 Programa de Doctorado en Ciencias Agroalimentarias, Facultad de Ciencias Agronómicas y de los Alimentos, Pontificia Universidad Católica de Valparaíso, Quillota 2340025, Quillota, Chile; laura.sepulveda@pucv.cl
5 Millennium Institute Center for Genome Regulation (CRG), Santiago 8320165, Santiago, Chile; victoria.lillo@agrigenomics.cl
6 Departamento de Biología, Facultad de Química y Biología, Universidad de Santiago de Chile, Santiago 9170022, Santiago, Chile; carlos.nunez.ma@usach.cl
7 Departamento de Fruticultura y Enología, Facultad de Agronomía y Sistemas Naturales, Pontificia Universidad Católica de Chile, Santiago 8331150, Santiago, Chile
8 Facultad de Ciencias Biológicas, Pontificia Universidad Católica de Chile, Santiago 8320000, Santiago, Chile
9 Escuela de Agronomía, Facultad de Ciencias, Ingeniería y Tecnología, Universidad Mayor, Huechuraba 8580745, Santiago, Chile
10 Facultad de Economía, Negocios y Gobierno, Universidad San Sebastián, Huechuraba 8580704, Santiago, Chile; frzambra@gmail.com
* Correspondence: andrea.miyasaka@umayor.cl
† These authors contributed equally to this work.

Abstract

Perennial deciduous trees such as *Prunus avium* undergo seasonal transitions, culminating in bud dormancy establishment that involves coordinated physiological and metabolic adjustments. Dormancy monitoring in orchard systems still relies primarily on temperature-based models and forcing assays, which rarely incorporate physiological or biochemical indicators. Here, we tested whether seasonal metabolic dynamics associated with dormancy progression differ between sweet cherry genotypes and whether these physiological differences are reflected in canopy-scale vegetation indices derived from satellite observations. Field measurements were conducted in two genotypes with contrasting chilling behavior ('Regina' and '210') during the transition from vegetative growth to dormancy. Leaf gas exchange and chlorophyll fluorescence were monitored across the season, polar metabolites in floral buds were profiled by gas chromatography-mass spectrometry, and satellite-derived vegetation indices were used to characterize canopy dynamics. Dormancy progression was associated with declines in CO_2 assimilation, transpiration, PSII photochemical efficiency, and electron transport rate, accompanied by increases in intercellular CO_2 concentration and non-regulated energy dissipation. Metabolomic analysis revealed that genotype explained a larger proportion of metabolite variation than dormancy stage (PERMANOVA R^2 = 0.483, p = 0.001), while principal component analysis accounted for 79.7% of total variance. Fructose showed the strongest genotype difference during paradormancy I, corresponding to an approximately 9.5-fold increase in 'Regina'. Pathway enrichment analysis highlighted starch and sucrose metabolism and pyruvate metabolism

Check for updates

Academic Editors: Songling Bai, Junkai Wu and Yuepeng Han

Received: 23 January 2026
Revised: 13 March 2026
Accepted: 26 March 2026
Published: 3 April 2026

Copyright: © 2026 by the authors. Licensee MDPI, Basel, Switzerland. This article is an open access article distributed under the terms and conditions of the Creative Commons Attribution (CC BY) license.

as the most represented pathways during dormancy progression. Satellite-derived vegetation indices captured seasonal canopy decline and were significantly associated with several physiological variables. These results provide an integrated description of physiological and metabolic adjustments during dormancy establishment in sweet cherry and highlight the potential of combining metabolomics, plant physiology, and open-access satellite observations to monitor phenological transitions in orchard systems at scalable spatial and temporal resolutions.

Keywords: phenology; metabolites; carbohydrates; remote sensing; photosynthesis

1. Introduction

Perennial deciduous fruit trees undergo seasonal cycles of growth, senescence, and dormancy that allow survival under unfavorable winter conditions. Dormancy is a complex physiological state characterized by the temporary suspension of visible growth while internal metabolic activity continues within buds and perennial tissues [1,2]. Classical conceptual frameworks distinguish paradormancy, endodormancy, and ecodormancy as sequential phases regulating bud development and growth competence in temperate woody species [3]. In sweet cherry (*Prunus avium* L.), dormancy progression and release are strongly influenced by winter chilling accumulation and environmental cues, making these processes highly sensitive to climatic variability [4]. Carbon metabolism plays a central role in dormancy regulation because buds depend on stored reserves to sustain maintenance respiration and support growth resumption in spring. Non-structural carbohydrates, including soluble sugars and organic acids, act both as energy sources and metabolic regulators, and their seasonal redistribution among perennial organs reflects physiological transitions associated with dormancy establishment and release [5].

Seasonal fluctuations in carbohydrate pools have been widely documented in woody perennials and are associated with cold acclimation, osmotic regulation, and metabolic maintenance during winter [6]. In sweet cherry flower buds, metabolomic analyses have revealed changes in compounds related to redox metabolism, carbohydrate pathways, and stress responses during dormancy progression, highlighting the importance of biochemical adjustments in bud physiology [7]. Recent advances in metabolomic approaches have improved the ability to characterize metabolic shifts associated with dormancy transitions in *Prunus* species. Untargeted metabolomic studies have identified candidate metabolites linked to oxidative metabolism, carbohydrate turnover, and secondary metabolic pathways as potential indicators of dormancy status in flower buds [8–10].

These biochemical patterns suggest that metabolite profiles could provide useful information for understanding the physiological regulation of dormancy and the readiness of buds to resume growth. In parallel, remote sensing technologies have emerged as powerful tools for monitoring plant physiological activity at the canopy scale. Vegetation indices derived from satellite imagery, particularly the normalized difference vegetation index (NDVI), have been widely used to assess canopy structure, photosynthetic activity, and seasonal vegetation dynamics [11]. Because these indices are closely related to leaf chlorophyll content, radiation absorption, and canopy density, they can provide indirect information about plant physiological status [12]. Remote sensing approaches have been successfully applied to characterize plant-water relations, transpiration dynamics, and phenological changes in agricultural systems [13–15]. However, the relationship between canopy scale spectral signals and biochemical processes occurring in dormant buds remains largely unexplored.

Genotypic variability represents another key factor influencing dormancy dynamics in sweet cherry. Different genotypes may exhibit contrasting chilling requirements, phenological timing, and carbon metabolism patterns during winter. In Chile, several sweet cherry accessions maintained in germplasm collections of the breeding programs have been characterized for genetic and phenotypic traits, including genotype '210' preserved at the INIA Los Tilos experimental station [16]. Therefore, the aim of this study was to characterize seasonal physiological and metabolic dynamics associated with dormancy progression in sweet cherry by integrating leaf gas exchange measurements, floral bud metabolite profiling, and satellite-derived vegetation indices. Particular emphasis was placed on comparing two sweet cherry genotypes, 'Regina' and genotype '210', to evaluate whether genotype-specific differences in carbon metabolism are reflected in canopy-scale spectral dynamics. We hypothesize that seasonal metabolic dynamics associated with dormancy progression differ between sweet cherry genotypes and that these physiological differences are reflected in canopy-scale vegetation indices derived from satellite observations.

Although metabolomic and physiological studies have provided insights into dormancy transitions in fruit trees, these approaches are typically conducted at the organ or tissue level and rarely integrated with canopy observations. Consequently, it remains unclear whether physiological and metabolic signals associated with dormancy progression can be detected using remote sensing approaches. Bridging these scales could provide new opportunities for monitoring dormancy dynamics in orchard systems using scalable technologies.

2. Materials and Methods

2.1. Study Design and Plant Material

From February to June 2017, physiological and phenological measurements were conducted on sweet cherry (*Prunus avium* L.) genotypes 'Regina' and '210' at the Instituto de Investigaciones Agropecuarias (INIA) Los Tilos Experimental Station located in Buin, Metropolitan Region, Chile (33°42′33.5″ S, 70°42′00.0″ W; 530 m a.s.l.) (Supplementary Figure S1). Genotype '210' corresponds to an advanced selection from the INIA Chile sweet cherry breeding program. Three five-year-old trees per genotype, grafted onto Cab-6p rootstocks, were selected within the same orchard block and monitored throughout the study period. The genotype 'Regina' is characterized by a relatively high chilling requirement [16], and the harvest date for the 2017 season was recorded on 17 December.

Phenological stages were defined based on seasonal progression, photoperiod changes, and the timing at which trees reached 50% leaf senescence (LS_{50}). Based on these criteria, three main phenological phases were established: vegetative growth (10 February–17 March; DOY 41-76), leaf senescence (18 March–4 May; DOY 77-124), and dormancy (5 May until LS_{50}; DOY 125-136). Phenological observations were recorded directly in the field during each sampling (Supplementary Table S1).

To evaluate dormancy progression, twigs were periodically collected during the autumn-winter period and subjected to forcing experiments. Dormancy status was assessed as the percentage of bud break observed after 14 days under controlled conditions (25 °C under a 16 h light/8 h dark photoperiod). Environmental conditions were monitored using meteorological data from the field station, and chilling accumulation was calculated as chill hours (CH) to evaluate the fulfillment of chilling requirements for each genotype.

2.2. Remote Sensing Indicators of Vegetation Activity

Vegetation indices were derived from multispectral imagery obtained through the Harmonized Landsat Sentinel (HLS) dataset, which integrates observations from two satellite programs. The Landsat missions, managed jointly by NASA and the U.S. Geological Survey (USGS), provide a long-term record of Earth observation, while the Sentinel-2A and

-2B satellites, operated under the European Commission's Copernicus Program, deliver high-resolution multispectral data [17].

For the 2017 season, imagery was obtained for the 'Regina' orchard at INIA Los Tilos. Two vegetation indices were calculated: the normalized difference vegetation index (NDVI) and the fraction of absorbed photosynthetically active radiation (FAPAR). NDVI was calculated from HLS imagery at a spatial resolution of 30 m using the red and near-infrared bands. FAPAR was derived from Sentinel-2 imagery using the Biophysical Processor implemented in SNAP version 9.0.0 https://step.esa.int/main/toolboxes/snap/ (accessed on 20 November 2022). A total of 41 cloud-free HLS scenes and 26 cloud-free Sentinel-2 scenes were available for analysis. For each dataset, curve fitting was applied to the vegetation index time series derived from all grove pixels to obtain smoothed trajectories and extract vegetation index values at the dates of the physiological assessments. Seasonal trajectories of NDVI and FAPAR were modeled using a double hyperbolic tangent function, following the approach described by Vrieling et al. [18]. This method enables detailed characterization of vegetation dynamics, including the timing and intensity of green-up and senescence phases.

2.3. Physiological and Photosynthetic Measurements

CO_2 assimilation rate (A), transpiration rate (E), stomatal conductance (g_s), and intercellular CO_2 levels (C_i) were measured using an infrared gas analyzer CI-340 (CID-Bioscience, Camas, WA, USA) [19]. Each leaf was measured four times on three branches per tree.

Fluorescence parameters were measured using a FluorPen FP 100 (Photon Systems Instruments, Drasov, Czech Republic). Measurements were taken from one leaf per tree, on three different branches, each covered for 30 min prior to measurement. A light curve was applied with 100, 200, 300, 500, and 1000 PAR, for 30 s each [20] (Supplementary Figure S2). The fluorometer exposed the leaf to modulated light (non-actinic) to determine the minimum fluorescence in darkness (F_0), followed by a saturating pulse to obtain the maximum fluorescence (F_m). Actinic light was applied to reach a steady state, and another saturating pulse was used to measure the maximum fluorescence adapted to light (F_m'). Fluorescence parameters were calculated as follows: $Y(II) = (F_m' - F_t)/F_m'$, for effective quantum yield of PSII (light absorbed by antenna complexes used to reduce plastoquinone) where F_t is the steady-state fluorescence in light, $Y(NPQ) = F_t/F_m' - F_t/F_m$ for quantum yield of regulated heat dissipation (excess energy released via the xanthophyll cycle), $Y(NO) = F_t/F_m$ for non-regulated heat dissipation (excess energy released as uncontrolled heat representing damage to the photosystems), and $ETR = Y(II) \times PAR \times 0.5 \times 0.84$, for the electron transport rate (electron flow through PSII) [21]. These measurements were always performed at 9:00 a.m., with weekly field visits during summer and autumn in the Southern hemisphere (from February to June 2017).

2.4. Sampling and Metabolomic Analysis of Floral Buds by Gas Chromatography–Mass Spectrometry (GC-MS)

Floral buds were collected from two sweet cherry genotypes, 'Regina' and '210', at three phenological stages between February and May 2017 (Figure 1). For each genotype, three trees were sampled as biological replicates, and three branches per tree were collected. Bud samples from each branch were pooled, and the average value per tree was used for statistical analyses. Sampling corresponded to three seasonal stages: a vegetative stage at DOY 45, a senescence stage at DOY 87, and the transition toward dormancy associated with 50% leaf senescence (LS_{50}). Immediately after collection, floral buds were flash frozen in liquid nitrogen, ground in ceramic mortars, and stored at −80 °C until processing. Samples

were then freeze-dried for 48 h and stored at −20 °C in hermetically sealed bags containing silica gel until metabolite extraction.

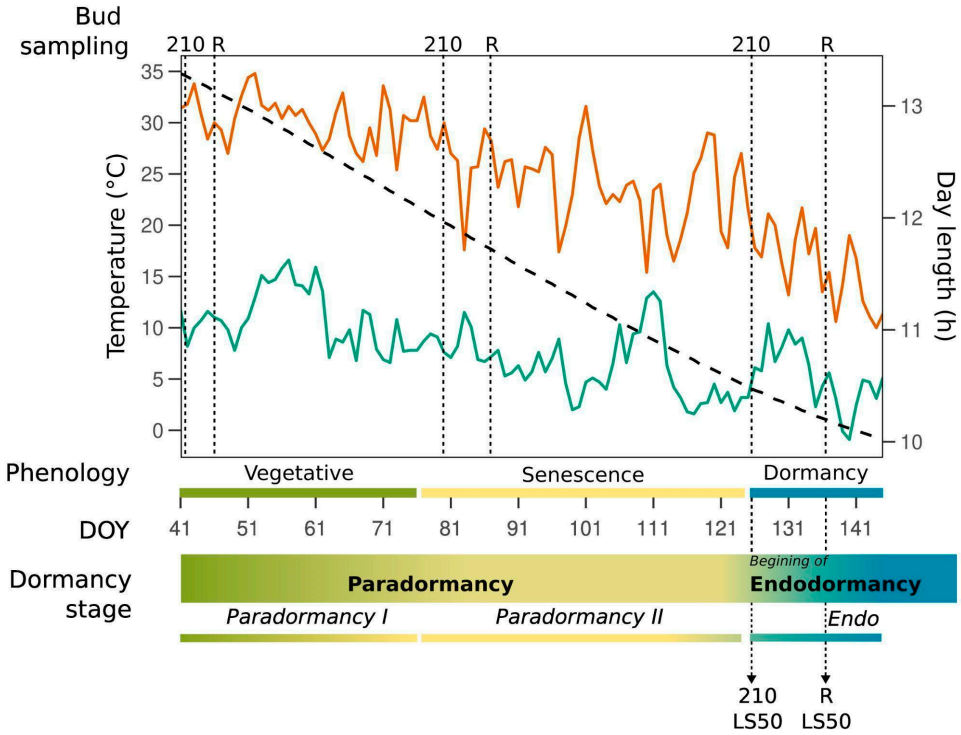


Figure 1. Seasonal framework of phenological events at the entrance of dormancy, environmental conditions, and sampling strategy in sweet cherry genotypes '210' and 'Regina' (R). Vegetative growth, senescence, and dormancy phases are indicated along the timeline, including paradormancy I, paradormancy II, and the onset of endodormancy. Vertical dashed lines indicate floral bud sampling dates for each genotype. The upper panel shows daily maximum (orange line) and minimum (green line) air temperatures (°C) and day length (black dashed line). The day of year (DOY) is shown on the x-axis, together with the corresponding phenological stages and dormancy phases. Arrows indicate the timing of 50% leaf senescence (LS_{50}) for genotypes '210' and 'Regina'.

2.5. GC-MS Polar Metabolite Analysis

Polar metabolite extraction followed Hatoum et al. (2014) [22], with minor modifications. Lyophilized floral buds (20 mg DW) were placed in 2 mL screw-cap tubes containing 500 µL of cold methanol and 20 µL of the internal standard solution. The internal standard (3000 ng/µL) was prepared by dissolving 3 mg of phenyl β-D-glucopyranoside (Sigma-Aldrich, St. Louis, MO, USA) in 1 mL of HPLC-grade methanol. Samples were incubated at 70 °C for 15 min at 1200 rpm and centrifuged at 15,000× *g* for 20 min. A 100 µL aliquot of the supernatant was transferred to 1.5 mL Eppendorf tubes and evaporated to dryness under a gentle nitrogen stream. The dried residues were resuspended in 120 µL of methoxylamine hydrochloride (20 mg/mL in pyridine) and incubated at 30 °C for 90 min at 1200 rpm. Subsequently, 120 µL of *N*,*O*-bis(trimethylsilyl)trifluoroacetamide (BSTFA; Sigma-Aldrich) was added, and samples were incubated at 37 °C for 30 min at 1200 rpm for derivatization. One microliter of each derivatized sample was injected in split mode (1:150) into a gas chromatograph (HP 6890 GC System; Agilent Technologies, Santa Clara, CA, USA) equipped with an HP-5ms capillary column (5% phenyl/95% dimethylpolysiloxane) and coupled to a 5973 Inert Mass Selective Detector (MSD) operating in electron impact mode. The injector was set at 220 °C, the transfer line at 280 °C, the ion source at 230 °C, and the quadrupole at 150 °C. Helium was used as a carrier gas at 1 mL/min. The MSD was operated with a scan range of 50–600 m/z and a scan rate of 2.66 scans/s. The oven program started at

120 °C (1 min), increased at 10 °C/min to 300 °C, and was held for 6 min. Chromatographic peaks were deconvoluted using AMDIS v.2.72 (Automated Mass Spectral Deconvolution and Identification System), and metabolite identification was performed by comparison of mass spectra with entries from the NIST mass spectral library. A pooled quality control (QC) sample was prepared by combining equal aliquots (100 µL) from each extract and processed under the same analytical conditions as the experimental samples; only metabolites detected in the QC sample and present in at least 70% of the biological samples were retained for further analysis. Relative metabolite abundance was calculated by normalizing metabolite peak areas to the internal standard (phenyl β-D-glucopyranoside) and to the dry weight of the analyzed tissue, and normalized values were further adjusted using the QC sample as a reference to account for potential analytical variation among injections.

2.6. Metabolic Pathway Analysis

Metabolic pathway analysis was performed using the Pathway Analysis module of MetaboAnalyst 6.0 [23]. Metabolites showing significant differences between genotypes across dormancy stages were mapped to metabolic pathways based on their Kyoto Encyclopedia of Genes and Genomes (KEGG) identifiers [24]. Pathway enrichment was evaluated using the GlobalTest algorithm and pathway topology using relative betweenness centrality to estimate pathway impact. The *Arabidopsis thaliana* pathway library was used as a reference because a curated KEGG pathway set for *Prunus avium* is not available in MetaboAnalyst. Pathways were interpreted considering both enrichment significance and pathway impact values.

2.7. Statistical Analyses

Physiological parameters (CO_2 assimilation, stomatal conductance, and chlorophyll fluorescence variables) were analyzed to evaluate differences among dormancy stages. Data normality and variance homogeneity were tested using the Shapiro Wilk and Levene tests, respectively. One-way analysis of variance (ANOVA) was applied to determine the effect of dormancy stage on each physiological variable, followed by Tukey's HSD post hoc test ($p \leq 0.05$) to identify significant pairwise differences. Correlation analyses between physiological parameters and selected metabolites were performed using Pearson's correlation coefficients to assess covariation patterns between photosynthetic performance and metabolite accumulation. Metabolomic data were further analyzed to assess variation between genotypes and dormancy stages. Metabolite abundances were averaged across branch pools within each tree, and trees were considered biological replicates (n = 3 per genotype × dormancy stage). Multivariate patterns among samples were examined using principal component analysis (PCA) on scaled metabolite data. Differences in metabolite profiles among dormancy stages and genotypes were evaluated using permutational multivariate analysis of variance (PERMANOVA) based on Euclidean distances, and homogeneity of dispersion was assessed using PERMDISP. Univariate comparisons of metabolite abundances between genotypes within each dormancy stage were performed using Student's *t*-tests, and *p*-values were adjusted for multiple testing using the false discovery rate (FDR) correction. Volcano plots were generated based on $\log_2$ fold change and FDR-adjusted *p*-values, and heatmaps representing relative metabolite abundances were constructed using mean values for each genotype × dormancy stage combination. For metabolic pathway analysis, pathways with $p < 0.05$ and pathway impact ≥ 0.1 were considered significantly perturbed [25], and figures were generated using the R packages ggplot2 and pheatmap.

Relationships between canopy spectral indices and leaf-level physiological variables were evaluated using linear regression models. For each physiological variable, models were fitted including the vegetation index (NDVI or FAPAR), genotype, and their interaction

term (Index × Genotype). This approach allowed assessment of both the overall association between spectral indices and physiological responses and potential differences in these relationships between genotypes.

Model coefficients and significance levels were extracted to evaluate the effects of the vegetation index, genotypes, and their interaction on each physiological variable. The coefficient of determination (R^2) was used to quantify the proportion of variance explained by each model. Significance thresholds of $p < 0.1$, $p < 0.05$, and $p < 0.01$ were used to identify marginally significant, significant, and highly significant effects, respectively.

For visualization, scatter plots with fitted linear regressions were generated for each genotype separately using the ggplot2 package, allowing graphical representation of genotype specific relationships between spectral indices and physiological variables.

3. Results

3.1. Phenological Events

Phenological stages of the trees were established based on the season, changes in photoperiod, and the date at which the trees had lost 50% of their leaves (LS_{50}), which were recorded at DOY 125 for genotype '210' and DOY 136 for 'Regina' (Figure 1). Differences in chill requirements were observed in these two genotypes, with 1041 CH and 1131 CH for '210' and 'Regina', respectively, along with dormancy release in the field, dated as DOY 237 for '210' and DOY 265 for 'Regina' (Supplementary Table S1).

3.2. Satellite-Derived Vegetation Indices Reveal Canopy Dormancy Signatures and Seasonal Recovery in Sweet Cherry

Remote sensing indicators of canopy activity, NDVI and FAPAR, exhibited clear seasonal dynamics that correspond to phenological transitions and dormancy-related changes in sweet cherry. Both indices reflect canopy greenness and light absorption efficiency and therefore serve as proxies for phenological stage and photosynthetic activity. The NDVI signal (Figure 2) remained high during summer and early autumn, reflecting maximal canopy greenness and active photosynthetic tissues. As the trees entered senescence, NDVI declined sharply, reaching minimum values between DOY 200 and 270, in line with the winter dormancy period. A rapid recovery was observed at the onset of spring, indicating synchronized budburst and canopy reactivation. Similarly, the FAPAR index, which quantifies the fraction of light absorbed by photosynthetically active vegetation, showed a progressive decline from early summer to winter (Figure 2). In contrast to NDVI, FAPAR exhibited an earlier and more pronounced decline at the beginning, reflecting a rapid reduction in the canopy's capacity to absorb photosynthetically active radiation. Minimum FAPAR values were recorded towards the end of winter, after which the index increased steadily, paralleling NDVI recovery toward DOY 300, aligning with the early stages of bud break and leaf expansion. NDVI-derived End of Season at 50% amplitude (EOS_{50}) occurred at DOY 137, closely matching the observed LS_{50} in 'Regina' (DOY 136) and occurring approximately 12 days later than LS_{50} in genotype '210' (DOY 125).

3.3. Seasonal Changes in Photosynthetic Performance and Gas Exchange

The physiological profiling of sweet cherry leaves across phenological stages revealed distinct seasonal trends in gas exchange dynamics that reflect the tree's metabolic adjustments during dormancy induction. Net photosynthetic assimilation rate (A) (Figure 3A) peaked during the early vegetative phase. As the season progressed, A showed a gradual decline, particularly evident during the leaf senescence phase, and reached minimum values during dormancy. Transpiration rate (E) followed a similar declining trend, with the highest rates observed during the vegetative phase (Figure 3C). As senescence advanced,

E decreased sharply and reached minimal values during dormancy, indicating a substantial reduction in water vapor exchange. Stomatal conductance (g_s) remained relatively low and stable during vegetative and senescence stages but exhibited a marked increase during dormancy (Figure 3D). Intercellular CO_2 concentration (C_i) displayed an opposite trend to A and E, increasing progressively in leaves during dormancy (Figure 3B). A decline in photosynthetic performance and gas exchange capacity was observed as dormancy established, with the increase in C_i coupled with declining A and E.

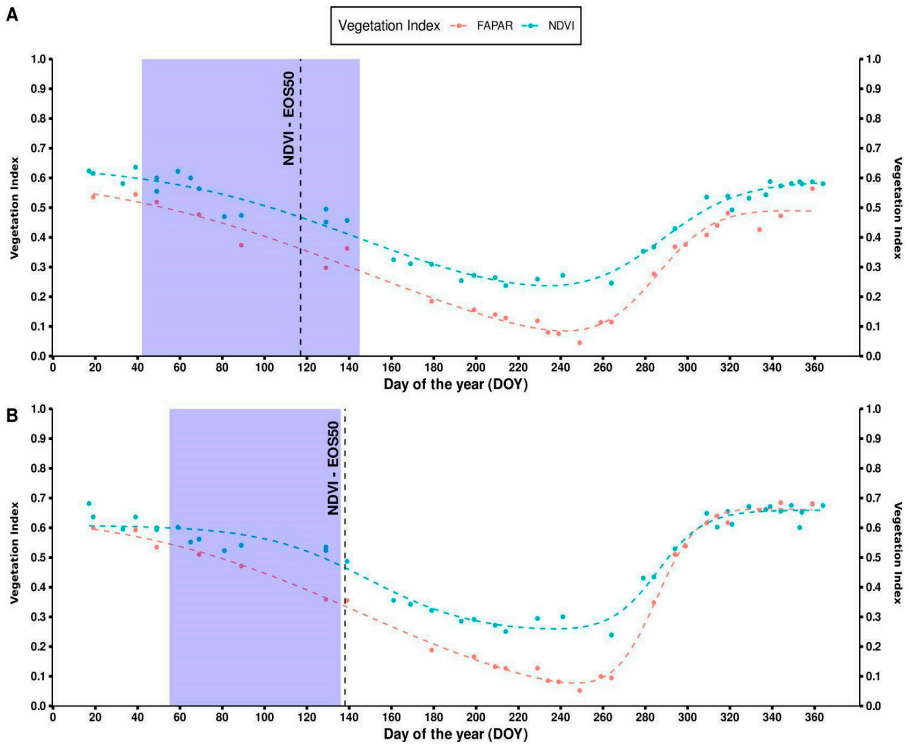


Figure 2. Seasonal trends in satellite-derived vegetation indices associated with canopy phenology in two sweet cherry genotypes: (**A**) '210' and (**B**) 'Regina'. Data points represent satellite-derived values at the orchard site, and the colored dashed curves indicate smoothed seasonal trends in the Normalized Difference Vegetation Index (NDVI, blue) and the Fraction of Absorbed Photosynthetically Active Radiation (FAPAR, red) across the annual cycle, expressed as days of the year (DOY). The purple shaded area indicates the period during which physiological measurements were performed. The vertical black dashed line indicates the NDVI-based End of Season at 50% amplitude (EOS50), defined as the DOY at which NDVI on the declining phase of the seasonal curve has decreased to half of its annual amplitude, marking the midpoint of canopy senescence.

3.4. Photosynthetic Efficiency and Electron Transport Activity Decline During Dormancy Onset in Sweet Cherry

Chlorophyll fluorescence analysis revealed marked seasonal shifts in photochemical performance of *Prunus avium* leaves, consistent with the progressive inactivation of photosystem II (PSII) during dormancy establishment (Figure 4). The effective quantum yield of PSII [Y(II)] showed the highest values during the vegetative phase but declined steadily through senescence, reaching minimal levels during dormancy (Figure 4A). This trajectory indicates a strong reduction in the efficiency of light energy conversion into photochemistry as photosynthetic capacity diminished. The electron transport rate (ETR) followed a similar trend, with maximum rates early in the season and a sharp decline during senescence and dormancy (Figure 4B). Both genotypes exhibited similar declines in Y(II) and ETR across the season, although 'Regina' maintained slightly higher values during early vegetative stages. This reduction highlights a substantial loss in the ability

of PSII to sustain electron flow under actinic light, reflecting a collapse in photochemical activity. By contrast, regulated non-photochemical quenching [Y(NPQ)], which represents photoprotective energy dissipation mechanisms, remained relatively high and stable across the season, with a slight increase during late senescence (Figure 4C). This suggests that even as photochemical utilization decreased, leaves maintained or enhanced their capacity to safely dissipate excess energy as heat, thereby minimizing photodamage under declining physiological activity. Non-regulated energy dissipation [Y(NO)] exhibited an opposite trajectory, remaining comparatively low during the vegetative phase but rising significantly during dormancy (Figure 4D). The increase in Y(NO) during the dormant stage indicates that a greater proportion of absorbed light energy was lost through non-regulated pathways, consistent with a breakdown of PSII control mechanisms once photosynthetic regulation is diminished.

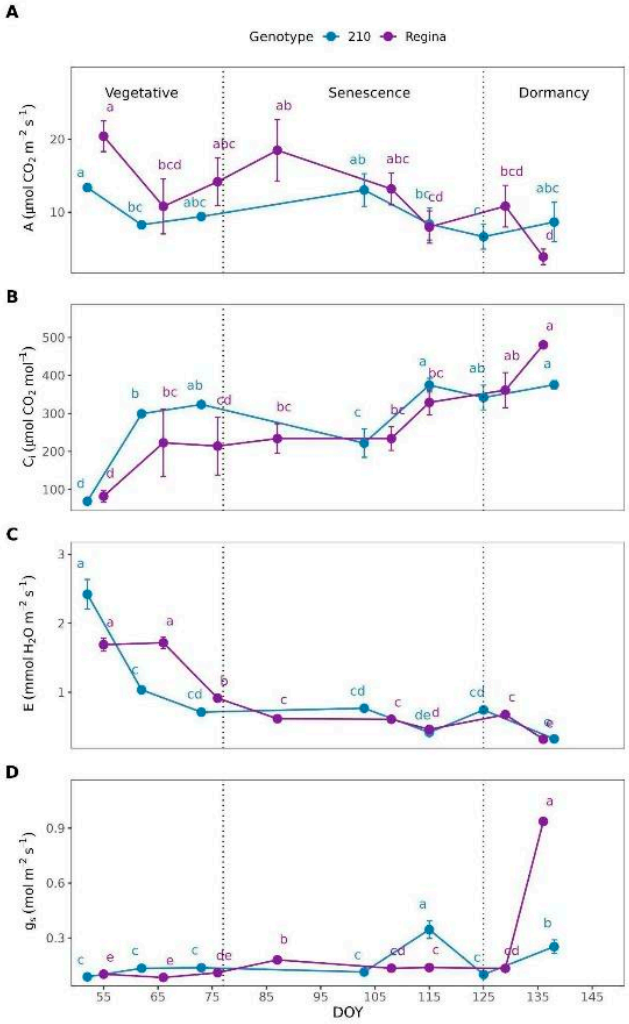


Figure 3. Seasonal dynamics of gas exchange parameters in the sweet cherry genotypes '210' and 'Regina' during the transition from vegetative growth to dormancy. Panels show (**A**) net CO_2 assimilation rate (A), (**B**) intercellular CO_2 concentration (C_i), (**C**) transpiration rate (E), and (**D**) stomatal conductance (g_s) measured in leaves across three phenological stages: vegetative growth, leaf senescence, and dormancy, indicated by vertical dashed lines. Genotype '210' in blue and 'Regina' in purple. Different letters above indicate statistically significant differences among sampling dates within each genotype (one-way ANOVA followed by Tukey's HSD test, $p \leq 0.05$). Data represent mean ± SE of biological replicates (n = 3 trees × 3 branches).

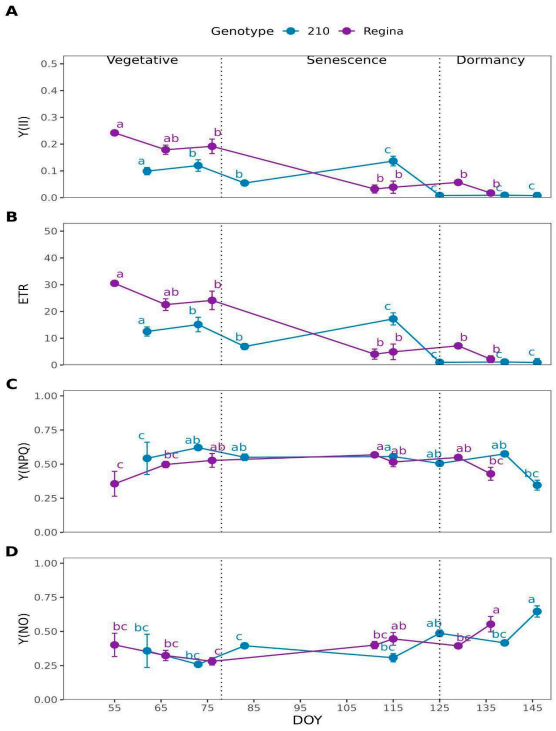


Figure 4. Seasonal variation in chlorophyll fluorescence parameters in *Prunus avium* leaves during dormancy. Panels show (**A**) effective quantum yield of PSII [Y(II)], (**B**) electron transport rate (ETR), (**C**) quantum yield of regulated non-photochemical energy dissipation [Y(NPQ)], and (**D**) non-regulated energy dissipation [Y(NO)] measured at a saturating actinic light intensity of 300 µmol photons m^{-2} s^{-1} (PAR). Measurements were collected across vegetative growth, leaf senescence, and dormancy stages indicated by vertical dashed lines. Blue symbols represent genotype '210' and purple symbols represent genotype 'Regina'. Different letters indicate significant differences among sampling dates within each genotype (one-way ANOVA with Tukey's HSD, $p \leq 0.05$). Data are mean ± SD (n = 3 trees × 3 branches).

3.5. Metabolite Profiles and Pathway Differences Between Genotypes Across Dormancy Stages

Relative metabolite abundance of five polar metabolites (fructose, glucose, malic acid, myo-inositol, and sorbitol) across dormancy stages and genotype is summarized in Supplementary Table S2. Two-way ANOVA detected significant genotype effects for fructose ($p = 4.88 \times 10^{-5}$, FDR = 2.44×10^{-4}), malic acid ($p = 4.02 \times 10^{-4}$, FDR = 1.01×10^{-3}) and myo inositol ($p = 0.025$, FDR = 0.042), whereas glucose and sorbitol were not significant after FDR correction. The dormancy stage and the interaction between genotype and dormancy stage were not significant after multiple testing corrections. Tukey comparisons indicated that the highest fructose values occurred in 'Regina' during paradormancy II, and the lowest values were observed in genotype '210' at the same stage (Table S2). Hierarchical clustering analysis showed genotype-related patterns of metabolite abundance across dormancy stages (Figure 5A). 'Regina' samples generally showed higher relative levels for several metabolites than genotype '210'. Fructose and sorbitol clustered together and showed the highest values in 'Regina' during paradormancy II, while malic acid showed higher levels in 'Regina' during endodormancy. Principal component analysis explained 79.7% of the total variance, with PC1 accounting for 54.9% and PC2 for 24.8% (Figure 5B). Samples were separated mainly according to genotype along PC1, with 'Regina' samples located on the positive side and genotype '210' on the negative side. Separation among dormancy stages along PC2 was limited, and samples from paradormancy II and endodormancy partially overlapped. PERMANOVA confirmed a significant effect of genotype on metabolite composition ($R^2 = 0.483$, $p = 0.001$), whereas dormancy stage was not sig-

nificant (R^2 = 0.157, p = 0.212) (Table S3). Tests of multivariate dispersion indicated no differences among groups (Treatment p = 0.959; Genotype p = 0.66). Volcano plot analysis within each dormancy stage showed a significant difference only for fructose during paradormancy I, where 'Regina' differed from genotype '210' (log_2FC = 3.25, FDR = 0.002), corresponding to an approximately 9.5-fold increase (Figure 5C; Table S4). Glucose, malic acid, myo-inositol, and sorbitol were not significant after correction, and no metabolites showed significant differences between genotypes during paradormancy II or endodormancy. Pathway enrichment analysis identified two metabolic pathways that met the criteria $p < 0.05$ and pathway impact ≥ 0.1: starch and sucrose metabolism (KEGG 00500) and pyruvate metabolism (KEGG 00620) (Figure 5D; Table S5). During paradormancy I, starch and sucrose metabolism showed an impact value of 0.316 (p = 0.0097) and pyruvate metabolism showed an impact value of 0.144 (p = 0.025). During paradormancy II, starch and sucrose metabolism showed an impact value of 0.316 ($p = 1.7 \times 10^{-5}$), and pyruvate metabolism showed an impact value of 0.144 ($p = 1.1 \times 10^{-4}$). During endodormancy, starch and sucrose metabolism showed an impact value of 0.300 (p = 0.029), and pyruvate metabolism showed an impact value of 0.144 (p = 0.020). These pathways were associated with fructose and glucose for starch and sucrose metabolism and with malate for pyruvate metabolism (Table S5).

Relationships between canopy spectral indices and leaf-level physiological variables were evaluated using linear models including genotype as a factor (NDVI × Genotype; Figure 6). Linear regression models revealed that NDVI explained a substantial proportion of the variability in several physiological variables (R^2 = 0.21–0.71). Significant NDVI effects were observed for Yield, Y(NO), Y(NPQ), ETR, E, and C_i, while genotype identity significantly influenced Yield, ETR, A, g_s, and C_i (Table 1). Across both genotypes, NDVI showed significant associations with several photosynthetic parameters, particularly electron transport rate (ETR), CO_2 assimilation rate (A), and PSII photochemical efficiency (Yield). In contrast, weaker relationships were observed for transpiration (E) and stomatal conductance (gs). Intercellular CO_2 concentration (Ci) exhibited a negative relationship with NDVI, indicating lower internal CO_2 levels at higher canopy vigor.

Table 1. Linear model results testing the relationship between NDVI and physiological parameters across genotypes.

Variable	R^2	NDVI	Genotype	NDVI × Genotype
Yield	0.71	***	***	***
Y(NO)	0.46	***	ns	ns
Y(NPQ)	0.21	**	.	*
ETR	0.71	***	***	***
g_s	0.48	ns	***	***
E	0.57	***	ns	ns
C_i	0.58	***	***	***
A	0.47	ns	***	***

Models were fitted as Variable ~ NDVI × Genotype. Significance levels: *** $p < 0.001$, ** $p < 0.01$, * $p < 0.05$, $p < 0.1$, ns = not significant.

The interaction between NDVI and genotype was significant for several variables, indicating that the strength of the NDVI–physiology relationship differed between genotypes. In particular, the genotype 'Regina' showed a steeper increase in photosynthetic activity with increasing NDVI than genotype '210'. Overall, these results indicate that canopy-level spectral indices capture meaningful variation in leaf-level physiological activity during the

seasonal transition toward dormancy, while also revealing genotype-specific differences in the coupling between canopy reflectance and photosynthetic performance.

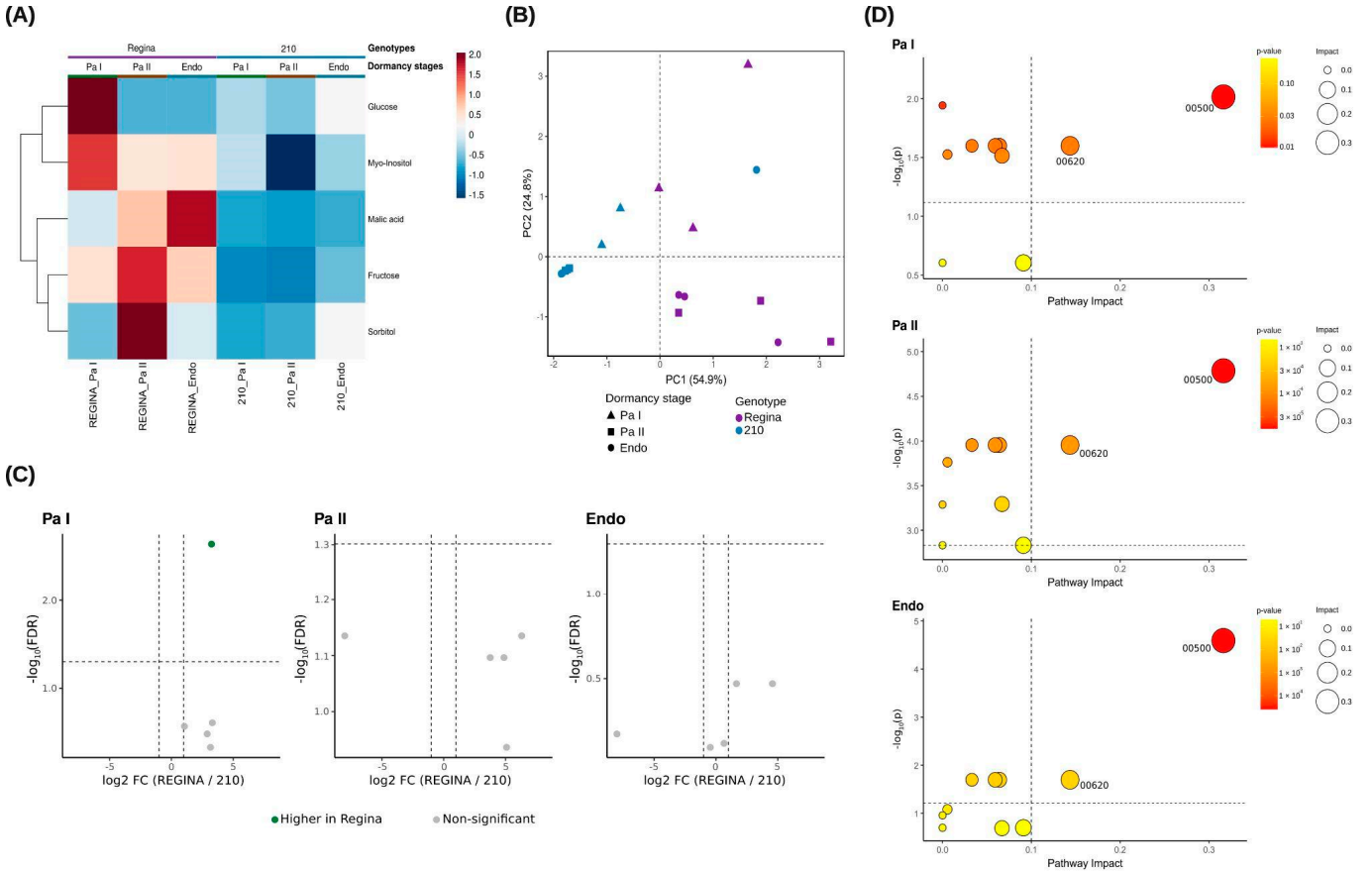


Figure 5. Multivariate analyses of metabolites in sweet cherry flower buds of the genotypes 'Regina' and '210' during paradormancy I (Pa I), paradormancy II (Pa II), and endodormancy (Endo). (**A**) Heatmap representation of the relative abundance of five carbon-related metabolites (fructose, glucose, malic acid, myo-inositol, and sorbitol) across genotypes and dormancy stages. Columns represent genotype × dormancy stage combinations, and values correspond to mean metabolite levels from three biological replicates (n = 3). The similarity measure used to cluster metabolites was based on Euclidean distance and Ward's linkage. (**B**) Principal component analysis (PCA) showing the distribution of metabolite profiles according to genotype and dormancy stage. Metabolite abundances were used as variables in the analysis. (**C**) Volcano plots showing metabolite differences between genotypes within each dormancy stage based on $\log_2$ fold change and FDR-adjusted *p*-values. The y axis represents −log10(FDR). Dashed horizontal lines indicate the significance threshold (FDR = 0.05), and dashed vertical lines indicate fold-change thresholds ($\log_2$FC = ±1). (**D**) Pathway analysis of metabolite changes across dormancy stages. Pathways were mapped using the *Arabidopsis thaliana* KEGG pathway library. The y axis represents −log10(*p*-values) derived from pathway enrichment analysis, and the x axis indicates pathway impact based on topology analysis. Dashed horizontal and vertical lines indicate the significance thresholds ($p = 0.05$ and pathway impact = 0.1, respectively), and pathways exceeding both thresholds were considered significantly affected. Numbers shown next to points correspond to KEGG pathway identifiers (i.e., 00500: starch and sucrose metabolism; 00620: pyruvate metabolism).

To evaluate whether these relationships were consistent across canopy spectral metrics, the same regression analyses were performed using the Fraction of Absorbed Photosynthetically Active Radiation (FAPAR) (Supplementary Figure S3; Supplementary Table S6). Similar patterns were observed, with FAPAR explaining a substantial proportion of the variability in several physiological variables (R^2 = 0.23–0.78). Significant FAPAR effects were

detected for Yield, Y(NO), Y(NPQ), ETR, E, and C_i, while genotype identity significantly influenced Yield, ETR, A, g_s, and C_i. As observed for NDVI, several variables showed significant FAPAR × Genotype interactions, indicating genotype-specific differences in the relationship between canopy spectral indices and physiological activity.

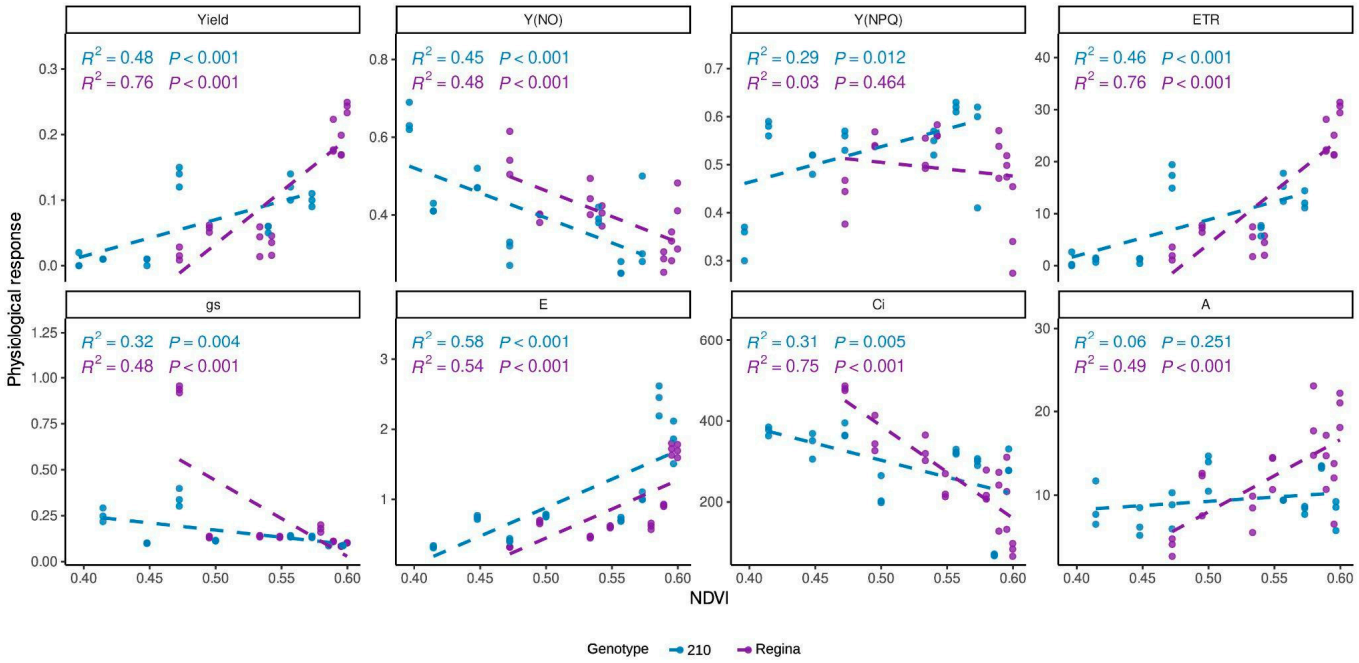


Figure 6. Relationships between canopy spectral signals and leaf-level physiological parameters during dormancy progression. Scatterplots show linear regressions between the Normalized Difference Vegetation Index (NDVI) and physiological variables measured at the leaf level: effective quantum yield of PSII (Yield, ΦPSII), non-regulated energy dissipation (Y(NO)), regulated heat dissipation (Y(NPQ)), electron transport rate (ETR), stomatal conductance (gs), transpiration rate (E), intercellular CO_2 concentration (Ci), and CO_2 assimilation rate (A). Data are shown separately for the two genotypes ('210' in blue and 'Regina' in purple). Dashed lines represent fitted linear models for each genotype. Coefficients of determination (R^2) and associated *p* values are displayed within each panel. These relationships illustrate how canopy-level spectral indices correspond to physiological processes associated with photosynthetic efficiency, energy dissipation, and gas exchange during dormancy transitions.

4. Discussion

The gradual decline in canopy function, leaf-level photosynthesis, and carbohydrate metabolism in flower buds observed in *Prunus avium* suggests that the onset of dormancy involves a coordinated whole-tree response to seasonal environmental cues. The timing of these changes, coinciding with shorter days and cooler temperatures, highlights the central role of environmental cues in dormancy induction, a concept well established in the literature on deciduous species [26] and supported by empirical findings on photothermal control in temperate fruit trees [27,28]. Leaf-level physiological measurements confirmed the systemic nature of this seasonal transition. Net CO_2 assimilation, stomatal conductance, and transpiration declined progressively from late summer through winter, while intercellular CO_2 concentration increased, suggesting that the reduction in photosynthetic capacity was primarily driven by non-stomatal, biochemically based limitations rather than by restricted CO_2 diffusion [29]. These patterns are consistent with the progressive decline in photosynthetic proteins such as Rubisco, together with chlorophyll loss during leaf senescence [30,31], as well as the redirection of carbohydrate fluxes from actively photosynthesizing tissues toward storage organs [32].

Chlorophyll fluorescence measurements supported these observations, revealing coordinated declines in photochemical efficiency and electron transport activity (Figure 4) as the season progressed. Dormancy induction was accompanied by reductions in PSII photochemical yield and electron transport rate, indicating a diminished capacity for photochemical energy conversion [33,34]. In contrast, non-photochemical quenching exhibited a transient peak, reflecting temporary activation of xanthophyll cycle-dependent thermal dissipation during senescence, which later declined as tissues lost functional integrity [35]. These trends parallel the seasonal reductions in gas exchange capacity (Figure 3), supporting the idea that dormancy induction involves reductions in both carbon assimilation and photochemical energy use, together with increased reliance on energy dissipation mechanisms to maintain leaf integrity under low metabolic demand. Similar seasonal adjustments in photosynthetic activity and energy partitioning have been reported in other deciduous species [36–38].

Metabolomic analyses revealed that genotype explained a larger proportion of variation in floral bud metabolite composition than dormancy stage. This result suggests that the metabolic profiles of 'Regina' and genotype '210' remain distinct throughout the evaluated dormancy phases. Similar genotype-dependent differences in winter carbohydrate metabolism have been reported in woody perennials, where genotype identity influences carbon storage, reserve mobilization, and maintenance metabolism during dormancy [39,40]. Among the analyzed metabolites, fructose showed the strongest genotype-specific signal, with significantly higher levels in 'Regina' during paradormancy I. Soluble sugars such as glucose and fructose are closely associated with carbohydrate remobilization and cold acclimation in temperate fruit trees [41,42], reflecting the degradation of starch reserves and the accumulation of readily available carbon substrates.

In addition to sugars, malic acid contributed to the metabolic differentiation between genotypes and was associated with the pyruvate metabolism pathway. Organic acids such as malate link carbohydrate metabolism with central carbon metabolism and may reflect differences in carbon allocation strategies among cultivars during dormancy establishment [43,44]. The enrichment of starch and sucrose metabolism and pyruvate metabolism pathways further supports the interpretation that genotype differences primarily involve carbohydrate turnover and central metabolic processes in dormant buds. However, these metabolite associations should not be interpreted as direct regulatory mechanisms, and broader metabolomic coverage combined with transcriptomic or physiological analyses will be necessary to clarify their functional role in dormancy regulation. Despite the relatively small number of trees included in this study, the experimental design captured seasonal physiological and metabolic dynamics through repeated measurements across branches and sampling dates. Nevertheless, dormancy responses in sweet cherry may vary among genotypes with different chilling requirements, environmental conditions, and rootstocks. Future studies including additional genotypes, orchard sites, and growing seasons will therefore be necessary to evaluate the broader applicability of these physiological and metabolic patterns.

Remote sensing metrics provided complementary insights into seasonal canopy dynamics during dormancy progression (Figure 2). Satellite-derived vegetation indices such as NDVI and FAPAR tracked the decline in canopy activity during autumn senescence and the subsequent recovery toward spring, reflecting changes in canopy photosynthetic capacity. NDVI showed a sharper decline during leaf senescence, whereas FAPAR exhibited a smoother seasonal trajectory, consistent with their different biophysical sensitivities: NDVI primarily responds to canopy chlorophyll content and greenness [45], while FAPAR quantifies the fraction of incoming photosynthetically active radiation absorbed by the canopy [46]. These seasonal trends indicate that satellite-derived spectral signals can

capture canopy-level phenological transitions and track physiological changes occurring during the progression from active growth to dormancy.

The association between canopy spectral signals and physiological measurements was further explored using linear regression models that included genotype effects (Figure 6; Table 1). NDVI explained a substantial proportion of the variability in several physiological variables ($R^2 \approx 0.21$–0.71) and showed significant relationships with key photosynthetic parameters, including electron transport rate (ETR), PSII photochemical efficiency (Yield), and transpiration (E). In contrast, the relationship between NDVI and CO_2 assimilation rate (A) differed between genotypes, as indicated by a significant NDVI × genotype interaction. Overall, higher canopy greenness was generally associated with greater photosynthetic activity at the leaf level. NDVI is widely used as an indicator of canopy greenness and photosynthetic activity because it is strongly influenced by chlorophyll content and canopy structure, which regulate light absorption by the photosynthetic apparatus. Similarly, the Fraction of Absorbed Photosynthetically Active Radiation (FAPAR) represents the fraction of incoming radiation absorbed by the canopy and is closely linked to photosynthetic processes and plant productivity. Previous studies have shown that spectral indices, such as NDVI, correlate with canopy photosynthesis and vegetation physiological status [47], supporting their use as indicators of vegetation functioning. Comparable patterns were observed when FAPAR was used as the explanatory variable (Supplementary Figure S3; Supplementary Table S6), further supporting the robustness of the relationships between canopy spectral metrics and leaf-level physiological activity. Conversely, intercellular CO_2 concentration (Ci) tended to decrease as NDVI increased, consistent with enhanced CO_2 assimilation under conditions of greater canopy vigor. Several models also showed significant NDVI × genotype interactions, indicating that the strength of these relationships differed between genotypes and suggesting that canopy reflectance–physiology coupling may vary depending on genetic background.

These statistical relationships support the interpretation that canopy-level spectral indices reflect physiological changes occurring during dormancy transitions, although the linkage remains indirect. Because physiological measurements were obtained at the leaf level, whereas spectral indices represent canopy-scale signals, the observed associations should be interpreted as correspondence rather than direct mechanistic coupling. Nevertheless, similar relationships between satellite-derived vegetation indices and physiological indicators have been reported in orchard systems, where Sentinel-2 indices correlate with plant water status and other physiological parameters in sweet cherry [48].

Finally, the phenological transition derived from NDVI (EOS_{50}) showed good agreement with the LS_{50} determined from field observations (Figure 1). For genotype '210', NDVI-based EOS_{50} occurred eight days earlier than the observed LS_{50} (DOY 117 vs. 125), whereas for 'Regina' the estimate differed by only two days (DOY 138 vs. 136), resulting in a mean absolute difference of approximately five days. In contrast, FAPAR estimates showed larger discrepancies from field observations. Despite these differences, both indices correctly captured the relative phenological timing between genotypes, with genotype '210' reaching leaf senescence earlier than 'Regina'. These results suggest that remotely sensed vegetation indices, particularly NDVI, can capture key seasonal transitions in canopy activity. However, additional validation across multiple years and sites will be required to confirm their robustness for phenological or dormancy modeling applications in sweet cherry orchards.

5. Conclusions

This study demonstrates that integrating plant physiology, metabolomic profiling, and satellite remote sensing provides a comprehensive framework for characterizing dormancy

progression in *Prunus avium*. Seasonal declines in photosynthetic performance, including reductions in CO_2 assimilation, PSII efficiency, and electron transport rate, were accompanied by shifts in energy dissipation patterns during the transition from vegetative growth to dormancy, although the magnitude of some responses differed between genotypes.

Metabolomic analyses revealed that genotypes explained a larger proportion of variation in floral bud metabolite composition than dormancy stage, indicating strong genotype dependent metabolic profiles. Among the detected compounds, fructose showed the clearest genotype-specific signal, with significantly higher levels in 'Regina' during paradormancy I. Additional metabolites involved in carbohydrate and central carbon metabolism, including glucose, sorbitol, malic acid, and myo-inositol, contributed to the metabolic differentiation between genotypes and were associated with the enrichment of starch and sucrose metabolism and pyruvate metabolism pathways.

At the canopy scale, satellite-derived vegetation indices successfully captured seasonal declines in canopy activity and showed significant relationships with several leaf physiological parameters. These results indicate that remotely sensed vegetation indices can reflect physiological processes associated with dormancy transitions, although the relationship between canopy spectral signals and leaf physiology remains indirect.

These findings highlight the value of combining physiological measurements, metabolomic data, and remote sensing observations to improve the monitoring of phenological transitions in perennial orchard systems. Satellite-derived vegetation indices provide a scalable and cost-effective alternative to traditional phenological assessments, which often rely on labor-intensive field observations and forcing assays. Because imagery from platforms such as Landsat and Sentinel is freely available and continuously collected, remote sensing offers a powerful resource for monitoring crop phenology at broader spatial and temporal scales. Future studies including additional genotypes, environments, and growing seasons will be necessary to validate the robustness of these indicators for dormancy monitoring in sweet cherry.

Supplementary Materials: The following supporting information can be downloaded at: https://www.mdpi.com/article/10.3390/horticulturae12040443/s1, Table S1: Phenological stages for sweet cherry (*Prunus avium* L.) genotypes '210' and 'Regina' during the 2017 growing season at the INIA Los Tilos Experimental Station (Buin, Chile). Phenological events include early vegetative development (green tip and bud break), flowering stages (flowering starts at 5% open flowers, full bloom at 50% open flowers, end of flowering, and petal fall), early fruit development (green ovary and fruit at 50% of final size), fruit ripening stages (color break), and harvest maturity. Chilling accumulation is expressed as chill hours (CH), calculated from field meteorological data and evaluated in relation to dormancy progression using forcing experiment assays; Table S2: Two-way ANOVA results for metabolite abundance across dormancy stages and genotypes. *p*-values were calculated for the effects of genotype (Genotype), dormancy stage (Treatment), and their interaction. False discovery rate (FDR) correction was applied to account for multiple testing; Table S3: Permutational multivariate analysis of variance (PERMANOVA) based on metabolite profiles. The analysis tested the effects of dormancy stage (Treatment), genotype (Genotype), and their interaction using 999 permutations; Table S4: Stage-specific comparisons of metabolite abundance between genotypes ('Regina' and '210') across dormancy stages based on volcano plot analysis; Table S5: KEGG pathways significantly perturbed between genotypes across dormancy stages under study; Table S6: Linear model results testing the relationship between FAPAR and physiological parameters across genotypes. Models were fitted as Variable ~ FAPAR × Genotype. Significance levels: *** $p < 0.001$, ** $p < 0.01$, * $p < 0.05$, . $p < 0.1$, ns = not significant; Figure S1: Location of the study site at the Experimental Station INIA Los Tilos (Buin, Metropolitan Region, Chile; 33.7° S, 70.7° W; 530 m a.s.l.). The aerial image shows the experimental sweet cherry orchards used in this study. The purple outlined area corresponds to the 'Regina' genotype plot (7300 m^2), and the blue outlined area corresponds to the '210' genotype

plot (1530 m^2). Measurements were conducted in these orchards between February and June 2017. Satellite image source: Google Earth.; Figure S2: Light response curves of the effective quantum yield of PSII [Y(II)] measured in leaves of sweet cherry genotypes (A) '210' and (B) 'Regina' across different days of the year (DOY). Curves show the response of Y(II) to increasing photosynthetically active radiation (PAR; 100–1000 µmol photons m^{-2} s^{-1}). Colors indicate the sampling dates (DOY). Points represent mean values, and error bars indicate the standard error of the mean of biological replicates (n = 3 trees × 3 branches); Figure S3: Relationships between canopy spectral signals and leaf-level physiological parameters during dormancy progression. Scatterplots show linear regressions between the Fraction of Absorbed Photosynthetically Active Radiation (FAPAR) and physiological variables measured at the leaf level: effective quantum yield of PSII (Yield, ΦPSII), non-regulated energy dissipation (Y(NO)), regulated heat dissipation (Y(NPQ)), electron transport rate (ETR), stomatal conductance (gs), transpiration rate (E), intercellular CO_2 concentration (Ci), and CO_2 assimilation rate (A). Data are shown separately for the two genotypes ('210' in blue and 'Regina' in purple). Dashed lines represent fitted linear models for each genotype. Coefficients of determination (R^2) and associated *p* values are displayed within each panel. These relationships illustrate how canopy-level spectral indices correspond to physiological processes associated with photosynthetic efficiency, energy dissipation, and gas exchange during dormancy transitions.

Author Contributions: Conceptualization, A.M.A.; Data curation, L.U. and J.G.-L.; Formal Analysis, G.M.S., L.U., L.S., J.G.-L., V.C. and V.L.-C.; Funding Acquisition, F.Z. and A.M.A.; Investigation, L.U., J.G.-L., C.N. and V.L.-C.; Methodology, J.G.-L. and F.Z., Project Administration, A.M.A.; Resources, F.Z. and A.M.A.; Software, J.G.-L.; Supervision, F.Z. and A.M.A.; Validation, G.M.S., L.S. and A.M.A.; Visualization, G.M.S., L.U., L.S. and J.G.-L.; Writing—Original Draft Preparation, G.M.S.; Writing—Review and Editing, G.M.S., L.S., J.G.-L., F.Z. and A.M.A. All authors have read and agreed to the published version of the manuscript.

Funding: This research was funded by Agencia Nacional de Investigación y Desarrollo (ANID/Chile), Fondo Nacional de Desarrollo Científico y Tecnológico (FONDECYT) grants 1230163 (A.M.A.) and 1240628 (V.L-C), ANID/ACT210007 (A.M.A. and F.Z.), ANID Doctorado Nacional/2024-21250976 (L.S.) and Universidad Mayor Doctoral scholarship (G.M.S.).

Data Availability Statement: The original contributions presented in this study are included in the article/Supplementary Material. Further inquiries can be directed to the corresponding author.

Acknowledgments: We thank Instituto de Investigaciones Agropecuarias de Chile (INIA) Los Tilos, for giving us access to their fields for sampling. We also thank José Manuel Donoso, INIA's sweet cherry breeding program, for providing information about sweet cherry genotypes' phenology.

Conflicts of Interest: The authors declare no conflicts of interest. The funders had no role in the design of the study; in the collection, analyses, or interpretation of data; in the writing of the manuscript; or in the decision to publish the results.

Abbreviations

The following abbreviations are used in this manuscript:

DOY	Day of the year
FAPAR	Fraction of absorbed photosynthetically active radiation
NDVI	Normalized difference vegetation index

References

1. Shurygin, B.; Konyukhov, I.; Khruschev, S.; Solovchenko, A. Non-Invasive Probing of Winter Dormancy via Time-Frequency Analysis of Induced Chlorophyll Fluorescence in Deciduous Plants as Exemplified by Apple (*Malus* × *domestica* Borkh.). *Plants* **2022**, *11*, 2811. [CrossRef]
2. Da Silveira Falavigna, V.; Guitton, B.; Costes, E.; Andrés, F. I Want to (Bud) Break Free: The Potential Role of DAM and SVP-Like Genes in Regulating Dormancy Cycle in Temperate Fruit Trees. *Front. Plant Sci.* **2019**, *9*, 1990. [CrossRef]

3. Lang, G.A.; Early, J.D.; Martin, G.C.; Darnell, R.L. Endo-, Para-, and Ecodormancy: Physiological Terminology and Classification for Dormancy Research. *HortScience* **1987**, *22*, 701. [CrossRef]
4. Campoy, J.A.; Darbyshire, R.; Dirlewanger, E.; Quero-García, J.; Wenden, B. Yield Potential Definition of the Chilling Requirement Reveals Likely Underestimation of the Risk of Climate Change on Winter Chill Accumulation. *Int. J. Biometeorol.* **2019**, *63*, 183–192. [CrossRef]
5. Keller, J.D.; Loescher, W.H. Nonstructural Carbohydrate Partitioning in Perennial Parts of Sweet Cherry. *J. Am. Soc. Hortic. Sci.* **1989**, *114*, 969–975. [CrossRef]
6. Davidson, A.M.; Le, S.T.; Cooper, K.B.; Lange, E.; Zwieniecki, M.A. No Time to Rest: Seasonal Dynamics of Non-Structural Carbohydrates in Twigs of Three Mediterranean Tree Species Suggest Year-Round Activity. *Sci. Rep.* **2021**, *11*, 5181. [CrossRef] [PubMed]
7. Baldermann, S.; Homann, T.; Neugart, S.; Chmielewski, F.; Götz, K.; Gödeke, K.; Huschek, G.; Morlock, G.E.; Rawel, H.M. Selected Plant Metabolites Involved in Oxidation-Reduction Processes during Bud Dormancy and Ontogenetic Development in Sweet Cherry Buds (*Prunus avium* L.). *Molecules* **2018**, *23*, 1197. [CrossRef]
8. Guillamón, J.G.; Prudencio, Á.S.; Yuste, J.E.; Dicenta, F.; Sánchez-Pérez, R. Ascorbic Acid and Prunasin, Two Candidate Biomarkers for Endodormancy Release in Almond Flower Buds Identified by a Nontargeted Metabolomic Study. *Hortic. Res.* **2020**, *7*, 203. [CrossRef]
9. Guillamón, J.G.; Andreu-Ardil, L.; Dicenta, F.; Ruiz, D.; López-Marqués, R.L.; Sánchez-Pérez, R. Investigating the Effect of Plant Growth Regulators in the Endodormancy Release in Apricot by a Metabolomic Approach. *J. Plant Growth Regul.* **2024**, *43*, 3795–3812. [CrossRef]
10. Guillamón, J.G.; Yuste, J.E.; López-Alcolea, J.; Dicenta, F.; Sánchez-Pérez, R. Unraveling Metabolic Shifts in Peach under Agrochemical Treatments during Flower Bud Endodormancy in the Context of Global Warming. *Front. Plant Sci.* **2025**, *16*, 1502436. [CrossRef]
11. Gamon, J.A.; Field, C.B.; Goulden, M.L.; Griffin, K.L.; Hartley, A.E.; Joel, G.; Penuelas, J.; Valentini, R. Relationships between NDVI, Canopy Structure, and Photosynthesis in Three Californian Vegetation Types. *Ecol. Appl.* **1995**, *5*, 28–41. [CrossRef]
12. Glenn, E.P.; Huete, A.R.; Nagler, P.L.; Nelson, S.G. Relationship between Remotely-Sensed Vegetation Indices, Canopy Attributes and Plant Physiological Processes: What Vegetation Indices Can and Cannot Tell Us about the Landscape. *Sensors* **2008**, *8*, 2136–2160. [CrossRef]
13. Alam, M.S.; Lamb, D.W.; Warwick, N.W.M. A Canopy Transpiration Model Based on Scaling up Stomatal Conductance and Radiation Interception as Affected by Leaf Area Index. *Water* **2021**, *13*, 252. [CrossRef]
14. Damm, A.; Paul-Limoges, E.; Haghighi, E.; Simmer, C.; Morsdorf, F.; Schneider, F.; Van der Tol, C.; Migliavacca, M.; Rascher, U. Remote Sensing of Plant–Water Relations: An Overview and Future Perspectives. *J. Plant Physiol.* **2018**, *227*, 3–19. [CrossRef] [PubMed]
15. Zhou, X.; Li, Y.; Luo, Y.; Sun, Y.; Su, Y.; Tan, C.; Liu, Y. Research on Remote Sensing Classification of Fruit Trees Based on Sentinel-2 Multi-Temporal Imageries. *Sci. Rep.* **2022**, *12*, 11549. [CrossRef] [PubMed]
16. Pizarro Véliz, M.A. Caracterización Genotípica y Fenotípica de una Colección de Cerezos (*Prunus avium* L.), con Énfasis en el Color y la Textura del Fruto. Master's Thesis, Universidad de Chile, Santiago, Chile, 2019.
17. Ju, J.; Zhou, Q.; Freitag, B.; Roy, D.P.; Zhang, H.K.; Sridhar, M.; Mandel, J.; Arab, S.; Schmidt, G.; Crawford, C.J.; et al. The Harmonized Landsat and Sentinel-2 Version 2.0 Surface Reflectance Dataset. *Remote Sens. Environ.* **2025**, *324*, 114723. [CrossRef]
18. Vrieling, A.; Meroni, M.; Darvishzadeh, R.; Skidmore, A.K.; Wang, T.; Zurita-Milla, R.; Oosterbeek, K.; O'Connor, B.; Paganini, M. Vegetation Phenology from Sentinel-2 and Field Cameras for a Dutch Barrier Island. *Remote Sens. Environ.* **2018**, *215*, 517–529. [CrossRef]
19. Volpe, G.; Lo Bianco, R.; Rieger, M. Carbon Autonomy of Peach Shoots Determined by 13C-Photoassimilate Transport. *Tree Physiol.* **2008**, *28*, 1805–1812. [CrossRef]
20. Baker, N.R. Chlorophyll Fluorescence: A Probe of Photosynthesis In Vivo. *Annu. Rev. Plant Biol.* **2008**, *59*, 89–113. [CrossRef]
21. Klughammer, C.; Schreiber, U. Complementary PSII Quantum Yields Calculated from Simple Fluorescence Parameters Measured by PAM Fluorometry and the Saturation Pulse Method. *PAM Appl. Notes* **2008**, *1*, 201–247.
22. Hatoum, D.; Annaratone, C.; Hertog, M.L.A.T.M.; Geeraerd, A.H.; Nicolai, B.M. Targeted Metabolomics Study of "Braeburn" Apples during Long-Term Storage. *Postharvest Biol. Technol.* **2014**, *96*, 33–41. [CrossRef]
23. Pang, Z.; Zhou, G.; Ewald, J.; Chang, L.; Hacariz, O.; Basu, N.; Xia, J. Using MetaboAnalyst 5.0 for LC–HRMS Spectra Processing, Multi-Omics Integration and Covariate Adjustment of Global Metabolomics Data. *Nat. Protoc.* **2022**, *17*, 1735–1761. [CrossRef]
24. Kanehisa, M.; Furumichi, M.; Sato, Y.; Kawashima, M.; Ishiguro-Watanabe, M. KEGG for Taxonomy-Based Analysis of Pathways and Genomes. *Nucleic Acids Res.* **2023**, *51*, D587–D592. [CrossRef] [PubMed]
25. Balic, I.; Olmedo, P.; Zepeda, B.; Rojas, B.; Ejsmentewicz, T.; Barros, M.; Aguayo, D.; Moreno, A.A.; Pedreschi, R.; Meneses, C.; et al. Metabolomic and Biochemical Analysis of Mesocarp Tissues from Table Grape Berries with Contrasting Firmness Reveals Cell Wall Modifications Associated to Harvest and Cold Storage. *Food Chem.* **2022**, *389*, 133052. [CrossRef] [PubMed]

26. Fadón, E.; Fernandez, E.; Behn, H.; Luedeling, E. A Conceptual Framework for Winter Dormancy in Deciduous Trees. *Agronomy* **2020**, *10*, 241. [CrossRef]
27. Heide, O.M.; Prestrud, A.K. Low Temperature, but Not Photoperiod, Controls Growth Cessation and Dormancy Induction and Release in Apple and Pear. *Tree Physiol.* **2005**, *25*, 109–114. [CrossRef]
28. Campoy, J.A.; Ruiz, D.; Egea, J. Dormancy in Temperate Fruit Trees in a Global Warming Context: A Review. *Sci. Hortic.* **2011**, *130*, 357–372. [CrossRef]
29. Flexas, J.; Medrano, H. Drought-Inhibition of Photosynthesis in C3 Plants: Stomatal and Non-Stomatal Limitations Revisited. *Ann. Bot.* **2002**, *89*, 183–189. [CrossRef]
30. Hörtensteiner, S. Chlorophyll Degradation during Senescence. *Annu. Rev. Plant Biol.* **2006**, *57*, 55–77. [CrossRef]
31. Zhu, X.-G.; Long, S.P.; Ort, D.R. What Is the Maximum Efficiency with Which Photosynthesis Can Convert Solar Energy into Biomass? *Curr. Opin. Biotechnol.* **2008**, *19*, 153–159. [CrossRef]
32. Loescher, W.H.; McCamant, T.; Keller, J.D. Carbohydrate Reserves, Translocation, and Storage in Woody Plant Roots. *HortScience* **1990**, *25*, 274–281. [CrossRef]
33. Murchie, E.H.; Lawson, T. Chlorophyll Fluorescence Analysis: A Guide to Good Practice and Understanding Some New Applications. *J. Exp. Bot.* **2013**, *64*, 3983–3998. [CrossRef] [PubMed]
34. Lichtenthaler, H.K.; Buschmann, C. Chlorophylls and Carotenoids: Measurement and Characterization by UV-VIS Spectroscopy. *Curr. Protoc. Food Anal. Chem.* **2001**, *1*, F4.3.1–F4.3.8. [CrossRef]
35. Demmig-Adams, B.; Adams, W.W., III. The Role of Xanthophyll Cycle Carotenoids in the Protection of Photosynthesis. *Trends Plant Sci.* **1996**, *1*, 21–26. [CrossRef]
36. Zuo, G. Non-Photochemical Quenching (NPQ) in Photoprotection: Insights into NPQ Levels Required to Avoid Photoinactivation and Photoinhibition. *New Phytol.* **2025**, *246*, 1967–1974. [CrossRef]
37. Arora, R.; Rowland, L.J.; Tanino, K. Induction and Release of Bud Dormancy in Woody Perennials: A Science Comes of Age. *HortScience* **2003**, *38*, 911–921. [CrossRef]
38. Chang, C.Y.-Y.; Bräutigam, K.; Hüner, N.P.A.; Ensminger, I. Champions of Winter Survival: Cold Acclimation and Molecular Regulation of Cold Hardiness in Evergreen Conifers. *New Phytol.* **2021**, *229*, 675–691. [CrossRef]
39. Sperling, O.; Zwieniecki, M.A. Winding up the Bloom Clock—Do Sugar Levels at Senescence Determine How Trees Respond to Winter Temperature? *Tree Physiol.* **2021**, *41*, 1906–1917. [CrossRef]
40. Tixier, A.; Gambetta, G.A.; Godfrey, J.; Orozco, J.; Zwieniecki, M.A. Non-Structural Carbohydrates in Dormant Woody Perennials; The Tale of Winter Survival and Spring Arrival. *Front. For. Glob. Change* **2019**, *2*, 18. [CrossRef]
41. Kaufmann, H.; Blanke, M. Changes in Carbohydrate Levels and Relative Water Content (RWC) to Distinguish Dormancy Phases in Sweet Cherry. *J. Plant Physiol.* **2017**, *218*, 1–5. [CrossRef]
42. Maurel, K.; Leite, G.B.; Bonhomme, M.; Guilliot, A.; Rageau, R.; Petel, G.; Sakr, S. Trophic Control of Bud Break in Peach (*Prunus persica*) Trees: A Possible Role of Hexoses. *Tree Physiol.* **2004**, *24*, 579–588. [CrossRef] [PubMed]
43. Marafon, A.C.; Citadin, I.; Amarante, L.D.; Herter, F.G.; Hawerroth, F.J. Chilling Privation during Dormancy Period and Carbohydrate Mobilization in Japanese Pear Trees. *Sci. Agric.* **2011**, *68*, 462–468. [CrossRef]
44. Zhuang, W.; Gao, Z.; Wen, L.; Huo, X.; Cai, B.; Zhang, Z. Metabolic Changes upon Flower Bud Break in Japanese Apricot Are Enhanced by Exogenous GA4. *Hortic. Res.* **2015**, *2*, 15046. [CrossRef]
45. Baret, F.; Guyot, G. Potentials and Limits of Vegetation Indices for LAI and APAR Assessment. *Remote Sens. Environ.* **1991**, *35*, 161–173. [CrossRef]
46. Zarco-Tejada, P.J.; González-Dugo, V.; Berni, J.A.J. Fluorescence, Temperature and Narrow-Band Indices Acquired from a UAV Platform for Water Stress Detection Using a Micro-Hyperspectral Imager and a Thermal Camera. *Remote Sens. Environ.* **2012**, *117*, 322–337. [CrossRef]
47. Badgley, G.; Field, C.B.; Berry, J.A. Canopy near-infrared reflectance and terrestrial photosynthesis. *Sci. Adv.* **2017**, *3*, e1602244. [CrossRef] [PubMed]
48. Zambrano, F.; Herrera, A.; Olguín, M.; Miranda, M.; Garrido, J.; Almeida, A.M. Prediction of the Daily Spatial Variation of Stem Water Potential in Cherry Orchards Using Weather and Sentinel-2 Data. *Agric. Water Manag.* **2025**, *318*, 109721. [CrossRef]

Disclaimer/Publisher's Note: The statements, opinions and data contained in all publications are solely those of the individual author(s) and contributor(s) and not of MDPI and/or the editor(s). MDPI and/or the editor(s) disclaim responsibility for any injury to people or property resulting from any ideas, methods, instructions or products referred to in the content.